Journal of ELECTRONIC MATERIALS, Vol. 45, No. 11, 2016
DOI: 10.1007/s11664-016-4811-z

Dielectric and Magnetic Properties of $Ba(Fe_{1/2}Ta_{1/2})O_3$-$BiFeO_3$ Ceramics

S. MANOTHAM,[1] P. BUTNOI,[1] P. JAITA,[1,2] S. PINITSOONTORN,[3] D. SWEATMAN,[1,2] S. EITSSAYEAM,[1,4] K. PENGPAT,[1,4] and G. RUJIJANAGUL[1,4,5]

1.—Department of Physics and Materials Science, Faculty of Science, Chiang Mai University, Chiang Mai 50200, Thailand. 2.—Science and Technology Research Institute, Chiang Mai University, Chiang Mai 50200, Thailand. 3.—Department of Physics, Faculty of Science, Khon Kaen University, Khon Kaen 40002, Thailand. 4.—Materials Science Research Center, Faculty of Science, Chiang Mai University, Chiang Mai 50200, Thailand. 5.—e-mail: rujijanagul@yahoo.com

The properties of $(1–x)Ba(Fe_{1/2}Ta_{1/2})O_3$-$xBiFeO_3$ [$(1–x)$BFT-xBFO] (x = 0.0, 0.1, 0.3, 0.5) ceramics have been investigated. $(1–x)$BFT-xBFO powders were synthesized by a modified two-step calcination technique, and ceramics were fabricated by a conventional technique. X-ray diffraction (XRD) analysis revealed that the modified ceramics exhibited a mixture of BFT cubic phase and BFO rhombohedral phase. The peaks shift increased with increasing BFO content to a maximum value for the composition with x = 0.5. The overall shift of the XRD patterns indicated distortion of the unit cell, which may be due to ions from BFO entering the BFT lattice. BFO additive promoted grain growth, while the maximum density of the studied ceramics was observed for the x = 0.1 composition. The modified ceramics presented enhanced thermal and frequency stability of the dielectric constant. BFO additive also reduced the loss tangent for the system. Improvement of the magnetic behavior was observed after adding BFO. Furthermore, all the ceramics, including pure BFT (a nonmagnetic phase at room temperature), presented a magnetocapacitance effect, which can be related to magnetoresistance along with Maxwell–Wagner polarization effects.

Key words: Dielectric, magnetic properties, magnetocapacitance, magnetoresistance

INTRODUCTION

High-dielectric-constant ceramics have been extensively studied due to their many potential electronic applications, e.g., in sensors and multilayer capacitors.[1–6] $Ba(Fe_{1/2}Ta_{1/2})O_3$ (BFT) is an interesting high-dielectric material since it shows a colossal dielectric constant. Many authors have reported that BFT presents cubic perovskite structure at room temperature (RT) in space group *Pm3m* (211)[2] and lattice parameter of 4.056 Å.[1,3] It has been reported that the dielectric constant of BFT ceramics varies from 10^3 to 10^5 over a wide temperature range (−150°C to 350°C).[2] The dielectric constant of BFT exhibits strong frequency dispersion, similar to other Fe-containing complex perovskite ceramics with composition $A(Fe_{1/2}B_{1/2})O_3$ (A = Sr, Ca, Ba; B = Nb, Ta, Sb).[1,4,5] Furthermore, BFT presents no ferroelectric properties.[2] Many modified BFT ceramics have been reported to show interesting properties compared with those of pure BFT, e.g., BFT-$Ba(Zn_{1/3}Ta_{2/3})O_3$[6] and $Ba_{1-x}Bi_x(Fe_{1/2}Ta_{1/2})O_3$[7] ceramics, which presented higher dielectric constants with lower loss tangents, and $Ba[(Fe_{0.9}Al_{0.1})_{1/2}Ta_{1/2}]O_3$ ceramics, which exhibited an extended giant dielectric constant with improved loss tangent. Furthermore, small amounts of $Ba(Fe_{1/2}Ta_{1/2})O_3$ produced a large shift of the peak

(Received May 4, 2016; accepted July 15, 2016; published online August 4, 2016)

in the dielectric constant–temperature curve for the $BaTiO_3$-$Ba(Fe_{1/2}Ta_{1/2})O_3$ system.[8]

For many years, multiferroic materials have been extensively investigated due to their many potential applications, e.g., in data storage, sensors, and memory devices.[9] However, multiferroic materials which exhibit both high ferromagnetic and ferroelectric properties are very rare, as ferromagnetism needs transition metals with unpaired 3*d* electrons and unfilled 3*d* orbitals, whereas ferroelectricity needs transition metals with filled 3*d* orbitals.[10] An interesting multiferroic material is bismuth ferrite $BiFeO_3$ (BFO), as it presents multiferroic properties at RT. BFO possesses rhombohedral symmetry (space group *R3c*)[11,12] with lattice parameters of $a = b = c = 0.3963$ Å and $\alpha = \beta = \gamma = 89.5°$ at RT.[13] Many authors have reported that BFO has a high Néel temperature (antiferromagnetic to paramagnetic transition temperature, $T_N \approx 370°C$) and high Curie temperature (ferroelectric to paraelectric transition temperature, $T_C \approx 830°C$).[14,15] However, BFO presents a low ferroelectric response, as it has high leakage current, which is reported to be due to formation of defects, such as oxygen vacancies, originating from reduction of Fe^{3+} to Fe^{2+}.[16] Furthermore, formation of secondary phases such as $Bi_2Fe_4O_9$ and $Bi_{25}FeO_{39}$ can also cause high leakage currents.[16–18] Many techniques have been proposed to improve the properties of BFO, such as doping BFO with various elements (e.g., Ba, Nb, Co)[19,20] or forming solid solution between BFO and other materials, e.g., $BiFeO_3$-$Ba_{0.85}Ca_{0.15}Ti_{0.90}Zr_{0.10}O_3$,[21] $BiFeO_3$-$PbTiO_3$,[22] $BiFeO_3$-$Ba(Zr_{0.6}Ti_{0.4})O_3$,[23] $Na_{0.5}Bi_{0.5}TiO_3$-$BiFeO_3$,[24] $BiFeO_3$-$BaTiO_3$,[25] and $BiFeO_3$-$Pb(Zr_{0.52}Ti_{0.48})O_3$.[26]

Since BFT presents a high dielectric constant over a wide temperature range and BFO is a multiferroic material at RT, it is interesting to form a new ceramic system between BFT and BFO with the aim of understanding its properties. However, the calcination temperature for BFT is high (1250°C) compared with BFO (850°C). Use of a conventional single-step calcination technique may result in problems when forming the (1–*x*)BFT-*x*BFO system, e.g., bismuth loss during processing (at higher calcination temperature) or incomplete reaction (at lower calcination temperature). Furthermore, many authors have reported that it is difficult to obtain a single phase of BFO by the conventional mixed-oxide technique.[27,28] Therefore, it is also difficult to prepare the (1–*x*)BFT-*x*BFO system by the conventional two-step calcination technique (synthesis of BFT and BFO separately, followed by mixing them together). This is because impurity phases may still be present in the samples. To ameliorate these problems, a modified two-step calcination technique was employed in this work, then (1–*x*)BFT-*x*BFO ceramics were fabricated by a conventional technique at a suitable sintering temperature. Many properties, such as the phase evolution, microstructure, and dielectric and magnetic properties, of all the ceramics were measured and investigated, and are discussed in detail herein.

EXPERIMENTAL PROCEDURES

(1–*x*)BFT-*x*BFO powders were prepared by a modified two-step calcination technique. For the first step, BFT powder was prepared by a solid-state reaction technique using $BaCO_3$, Fe_2O_3, and Ta_2O_5 as raw oxide materials. $BaCO_3$, Fe_2O_3, and Ta_2O_5 powders were mixed by ball-milling for 24 h in ethanol. The obtained powder was dried, then calcined at 1250°C for 6 h. For the second step, BFT powder was mixed with Bi_2O_3 and Fe_2O_3, according to the stoichiometry of the chemical formula (1–*x*)BFT-*x*BFO with $x = 0.0$, 0.1, 0.3, and 0.5. The mixed powders were milled again for 24 h, and calcined at 800°C for 2 h. A few drops of 4 wt.% polyvinyl alcohol (PVA) binder were then added to the calcined powders before being uniaxially pressed into 10-mm-diameter discs. To avoid the melting problem, ceramics for each condition were sintered at various temperatures below the melting temperature. In this work, ceramics with composition $x = 0.0$, 0.1, 0.3, and 0.5 were sintered for 2 h at optimum temperatures of 1450°C, 1200°C, 1100°C, and 1000°C, respectively. Ceramic samples were then selected for investigation of properties.

Phase formation of ceramics was characterized by x-ray diffraction (XRD) analysis. The density of the sintered ceramics was measured using the Archimedes method with distilled water as medium. The microstructure of the samples was investigated by scanning electron microscopy (SEM). For electrical measurements, two parallel surfaces of the sintered ceramic were polished, then silver paste was applied onto the polished surfaces of each sample. To form good electrodes, the resulting samples were then fired at 600°C for 15 min. Dielectric measurements as a function of temperature were carried out using an impedance analyzer (Agilent 4192A) at various frequencies. The ferroelectric properties at RT were examined using a ferroelectric tester (Radiant Technologies Inc.). The magnetic properties were obtained using vibrating-sample magnetometry (VSM, model 7404; Lake Shore Cryotronics, Inc., Westerville, OH) in magnetic field of $-10\ \text{kOe} \le H \le 10\ \text{kOe}$.

RESULTS AND DISCUSSION

Figure 1 presents the x-ray diffraction (XRD) patterns of the studied ceramics. For the unmodified ceramic ($x = 0.0$), pure perovskite phase was observed with no evidence of any impurity phase. The unmodified ceramic (BFT) presented cubic symmetry at RT, and XRD analysis was carried out based on International Centre for Diffraction Data (ICDD) file no. 01-089-2966. This XRD result also corresponds to the results of many previous authors for BFT ceramic.[1,29] For the modified ceramics ($x \ge 0.1$), BFO according to ICDD file no.

01-086-1518 (indicated by "◆" in the XRD patterns of Fig. 1) was observed. This indicates that the modified ceramics exhibited a mixture of BFT cubic phase and BFO rhombohedral phase. It should be noted that other impurity phases such as $Bi_{25}FeO_{39}$,[13,30] $Bi_{46}Fe_2O_{72}$,[13,31] and Bi_2O_3,[13,32] which are often observed in BFO, could not be detected in this work. Furthermore, the positions of all peaks were shifted slightly towards higher 2θ angle in comparison with the unmodified ceramic. This peak shift increased with increasing BFO content to a maximum value for the composition with $x = 0.5$. This overall shift of the XRD patterns indicates distortion of the unit cell, which may be due to ions from BFO entering the BFT lattice.

Figure 2a–c shows the surface morphology of (1–x)BFT-xBFO ceramics as revealed by SEM. The porosity level in the samples was consistent with the measured density; i.e., the $x = 0.1$ ceramic exhibited a quite dense form, while the other ceramics presented higher porosity. Microstructural investigation also indicated that BFO addition resulted in an increase in grain size. According to the average grain size values, as determined from the linear intercept method, the grain size value increased from ~1.3 μm for the unmodified ceramic to ~8.1 μm for the $x = 0.5$ ceramic (Fig. 2d). This data is in good agreement with literature reports;[21] i.e., an increased amount of BFO produced an increase in grain size value. However, our result is not consistent with the work done by Chao et al.,[33] who prepared the (1–x)[$(K_{0.458}Na_{0.542})_{0.96}Li_{0.04}$]$(Nb_{0.85}Ta_{0.15})O_3$-$x$BFO system using a conventional mixed-oxide method, where the grain size of the ceramics decreased with increasing BFO concentration. Furthermore, in their work, a higher amount of BFO also produced many large pores and inhomogeneous microstructure, which was related to the abnormal grain growth behavior. In the present work, however, the coarser grains for the ceramics containing higher amounts of BFO can be linked to formation of a liquid phase which can assist grain growth.

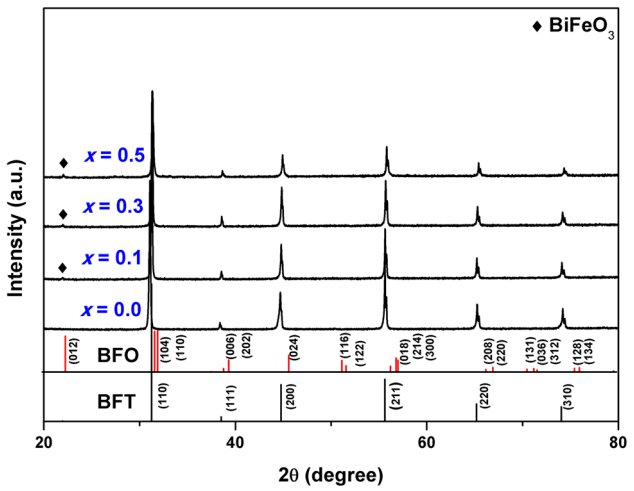

Fig. 1. XRD patterns of (1–x)BFT-xBFO ceramics for $2\theta = 20°$ to 80°.

Figure 2d shows the measured density as a function of BFO concentration. This data clearly shows that BFO addition influenced the ceramic density. The unmodified ceramic had a density of 7.32 g/cm^3. The density value increased to a maximum of 7.55 g/cm^3 for the $x = 0.1$ composition, then decreased to a minimum value of 7.29 g/cm^3 for the composition with $x = 0.5$. In this work, liquid-phase sintering may occur in the modified ceramics, as suggested by Chao et al.,[33] as BFO has a low melting point (~930°C). A suitable amount of liquid phase may assist the sintering process and result in the higher density for the $x = 0.1$ ceramic. The lower densities for the ceramics containing higher BFO concentrations ($x > 0.1$) may be because these ceramics were sintered at lower sintering temperatures. Also, a large amount of liquid phase (BFO) may produce an initial rapid densification but lower final density, as a result of void formation due to evaporation of BFO. This can result in high porosity of the pellets, which is not eliminated after the sintering process.

The dielectric constant (ε_r) as a function of temperature for the samples with different BFO concentrations is shown in Fig. 3. Unmodified BFT ceramic presented high dielectric constant, especially in the lower frequency region. The ε_r values tended to increase with increasing temperature, reaching a peak at high temperature (e.g., $\varepsilon_r \approx$ 129,500 at 270°C and 1 kHz). The dielectric constant dramatically decreased with increasing frequency, indicating that the dielectric constant of BFT ceramics exhibits very strong frequency dispersion. This behavior is similar to that reported in previous work for BFT ceramics.[2] In many cases, for high-dielectric ceramics, the very high dielectric constant can be linked to formation of oxygen vacancies.[34–36] Furthermore, formation of Fe^{2+}/Fe^{3+} has been proposed for ceramics containing Fe ions where the dielectric behavior of such ceramics has been linked to an electron hopping mechanism,[34,37] and formation of Fe^{2+}/Fe^{3+} can be promoted at high temperature.[35] Therefore, the very high dielectric constant for the BFT ceramics may be due to these effects.[34–38] With increasing BFO content, lower and broader dielectric constant curves were observed. Ceramics containing higher amounts of BFO presented improved dielectric constant–frequency stability compared with BFT ceramic, especially for the $x = 0.3$ and 0.5 samples. However, the dielectric constant for the $x = 0.5$ sample was still high ($\varepsilon_r \approx$ 3660 to 22,600 for 30°C to 350°C). It should be noted that samples with higher BFO content were sintered at lower sintering temperatures. Therefore, the lower dielectric constants with broader curves observed for the modified BFT ceramics may be because these ceramics were sintered at lower temperatures

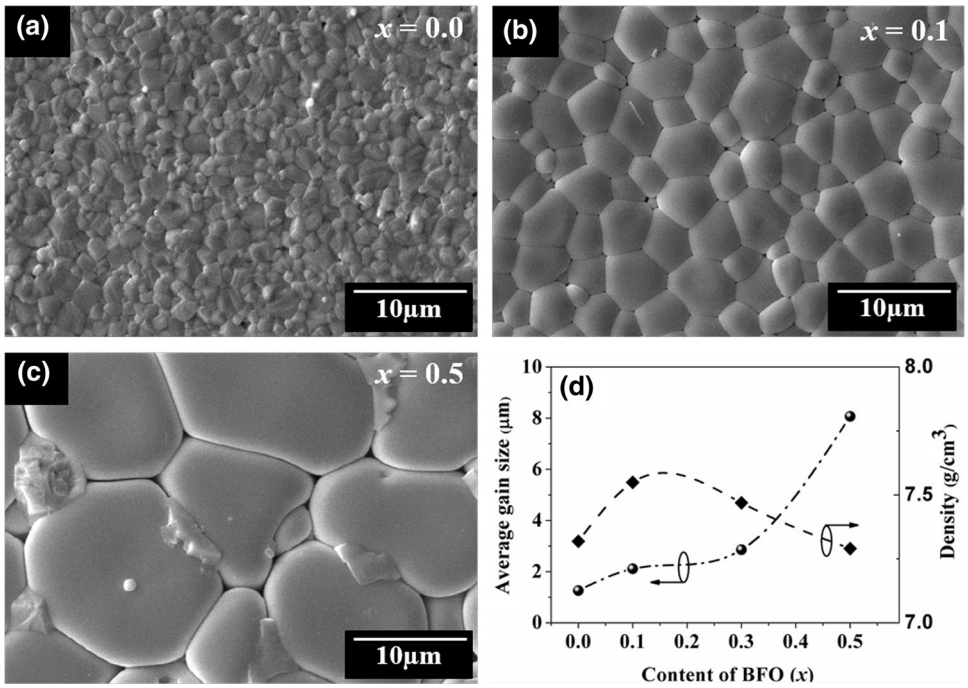

Fig. 2. (a–c) Selected SEM micrographs of studied ceramics with x = 0, 0.1, and 0.5. (d) Average grain size and density as functions of BFO content.

compared with the unmodified ceramic, resulting in a lower density. Lower sintering temperature could result in lower concentration of oxygen vacancies and Fe^{2+}/Fe^{3+} in the modified ceramics. These vacancies may contribute to the dielectric behavior observed for the modified ceramics. In addition, the heterogeneous composition of the samples with added BFO is considered to be another reason for these behaviors, as the modified ceramics contained a mixture of phases.

Plots of the loss tangent (tan δ) as a function of temperature at various frequencies for the x = 0.0 to 0.5 ceramics are shown in Fig. 4. The unmodified BFT ceramic exhibited high tan δ values with strong frequency dispersion. However, the tan δ values tended to decrease with increasing BFO content. The tan δ values decreased slightly for the x = 0.1 ceramic, then obviously for the x = 0.3 to 0.5 ceramics. Plots of tan δ as a function of temperature for the x = 0.0 to 0.5 ceramics at 1 kHz are displayed in the inset of Fig. 4. The tan δ value for the unmodified ceramic reduced from 3.12 to 1.07 for temperatures from 30°C to 200°C. These values are close to those reported in previous works.[2,29] After adding BFO, however, the tan δ values clearly decreased throughout the measurement temperature range. For example, the tan δ (at RT and 1 kHz) sharply decreased from 3.12 for the x = 0.0 ceramic to 0.26 for the x = 0.1 ceramic, then slightly decreased to 0.24 for the x = 0.5 ceramic. These results indicate that BFO helped to improve the tan δ behavior of the studied ceramics. Since the modified ceramics exhibited a mixture of phases, the tan δ behavior may be linked to the loss tangent of both the BFO and BFT phases. Therefore, a reason for the improvement of the tan δ value for the modified ceramics is that the BFO phase has a lower tan δ value (~0.15 to 0.4 at RT)[12] compared with the BFT phase (tan $\delta \sim$ 0.5 to 1 at RT).[2]

Figure 5 shows the polarization versus electric field (P–E) hysteresis loops at RT for ceramics containing different BFO concentrations. The hysteresis loop for the BFT ceramic presented a very large, rugby-ball-like loop, suggesting that this composition has high conductivity. This result also confirms that BFT ceramic exhibits nonferroelectric behavior at RT. Combining this result with the dielectric results (dielectric constant and loss tangent) suggests that BFT ceramic should be a material which exhibits relaxor-like dielectric behavior,[5,6] and the presence of frequency dependence of the dielectric constant in the present work is probably because the ceramics had heterogeneous electrical conduction, e.g., bulk grain and grain boundary had different electrical conduction.[39] Therefore, the dielectric behavior in this work should be explained by the Maxwell–Wagner mechanism, which can be related to a difference in the Fermi levels between different conduction regions.[6,40] After adding BFO, however, there was a transformation from the large rugby-ball-like loop to slim hysteresis loops (with increasing BFO content). Furthermore, the x = 0.5 ceramic presented a very slim, ferroelectric-like loop. This characteristic agrees with those reported in many previous works for BFO ceramics.[12,41] To check the

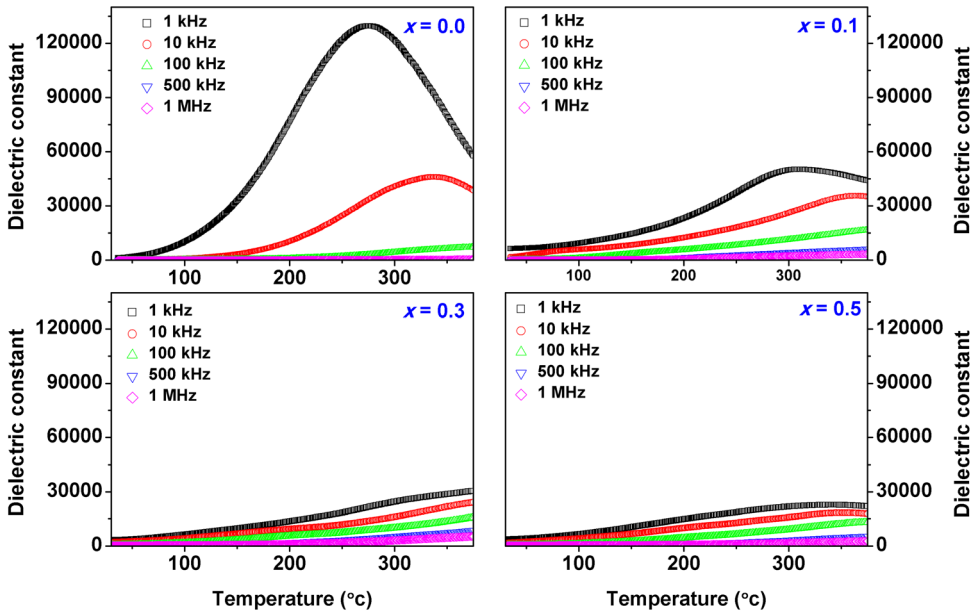

Fig. 3. Dielectric constant as function of temperature at various frequencies for x = 0.0 to 0.5 ceramic samples.

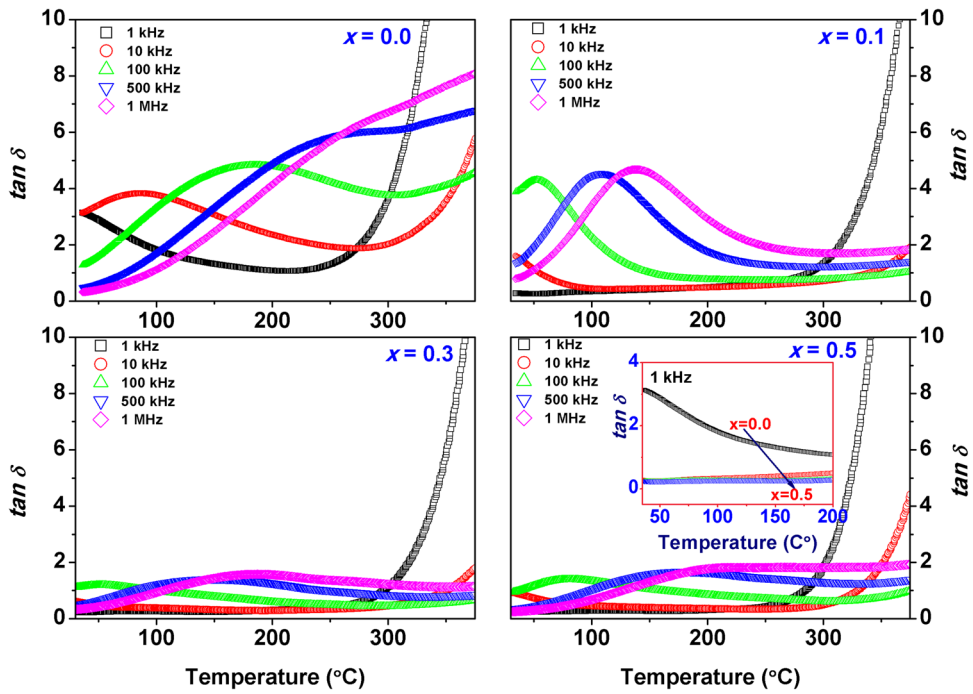

Fig. 4. Loss tangent as function of temperature at various frequencies for x = 0.0 to 0.5 ceramic samples. Inset shows loss tangent versus temperature for x = 0.0 to 0.5 ceramics at 1 kHz.

domain switching under applied electric fields, current–electric field (I–E) loops were also obtained (Fig. 5). The I–E characteristic loops for all ceramics seemed not to exhibit domain switching.[42] For the x = 0.5 ceramic, it was also difficult to confirm evidence of domain switching, since the ceramic broke down at low electric field (the maximum electric field for the x = 0.5 ceramic was 1.0 kV/cm).

Plots of magnetization (M) versus magnetic field (H) for the (1–x)BFT-xBFO ceramics, measured at RT, are shown in Fig. 6. It was found that the unmodified ceramic presented nonmagnetic behavior [inset (a) of Fig. 6]. However, improved magnetic properties were observed for the modified BFT ceramics, especially for the x = 0.5 ceramic. The remanent magnetization (M_r) and magnetic field (H_c) values were found to increase with increasing

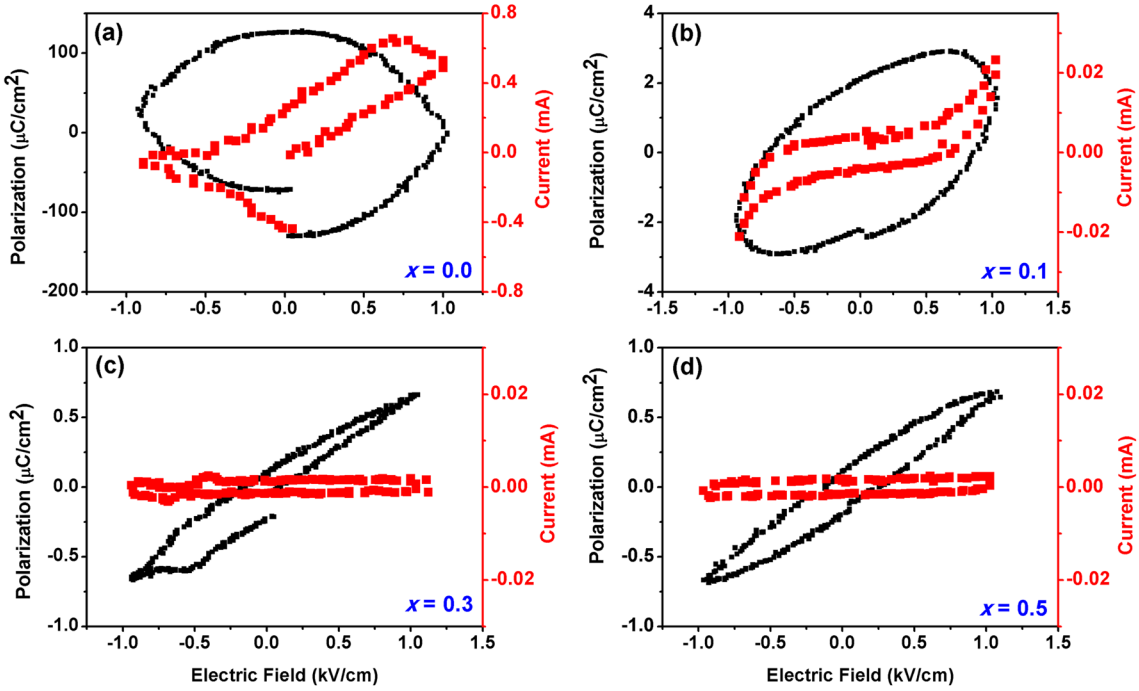

Fig. 5. *P–E* and *I–E* loops for (1–*x*)BFT-*x*BFO ceramics with (a) $x = 0.0$, (b) $x = 0.1$, (c) $x = 0.3$, and (d) $x = 0.5$.

BFO fraction. The M_r value increased from ~0 emu/g for the unmodified ceramic to ~0.26 emu/g for the $x = 0.5$ ceramic. The improved magnetic behavior of the modified ceramics may be due to the greater amount of magnetic ions with increasing BFO content.[43] In this work, the magnetic moment of the ceramics in terms of Bohr magnetons was calculated via the expression $\mu_B = (M \times \sigma'_S)/5585$, where μ_B is the Bohr magneton, M is the molecular weight for the particular composition, σ'_S represents the magnetization per gram mol of the sample, and 5585 is the magnetic fraction constant. The value of μ_B increased with increasing BFO concentration; i.e. magnetic ordering increased with increasing BFO content [inset (b) of Fig. 6]. This trend also agrees with many previous works on multiferroic composites.[44]

In the present work, the effect of an applied magnetic field on the ε_r value was also studied at RT. The frequency dependence of ε_r under an applied magnetic field for the studied samples is shown in Fig. 7. A change in the ε_r value under the applied magnetic field was observed. The magneto-capacitance (MC) at 100 Hz was calculated via the following equation: $\mathrm{MC} = \frac{[\varepsilon(H)-\varepsilon(0)]}{\varepsilon(0)} \times 100\%$, where $\varepsilon(H)$ is the dielectric constant under an applied magnetic field and $\varepsilon(0)$ is the dielectric constant without an applied magnetic field. The MC value versus the concentration x is displayed in Fig. 7d. The negative MC value increased with increasing BFO amount, suggesting that BFO additive affected the MC of all the ceramics. It should be noted that the applied magnetic field also influenced the ε_r value of the unmodified ceramic (a nonmagnetic phase at RT). Z^* (Z'–Z'') plots for the studied ceramics are shown in the insets of Fig. 7. Two arcs were observed in the Z^* plots for all the ceramics. This result indicates that all the ceramics exhibited heterogeneous conduction. For the unmodified ceramic, the Z^* plot presented an arc at high frequency, overlapping with another arc in the low frequency region without intercept. The arcs in the high and low frequency regions can be linked with the bulk grain and grain boundary responses, respectively.[29]

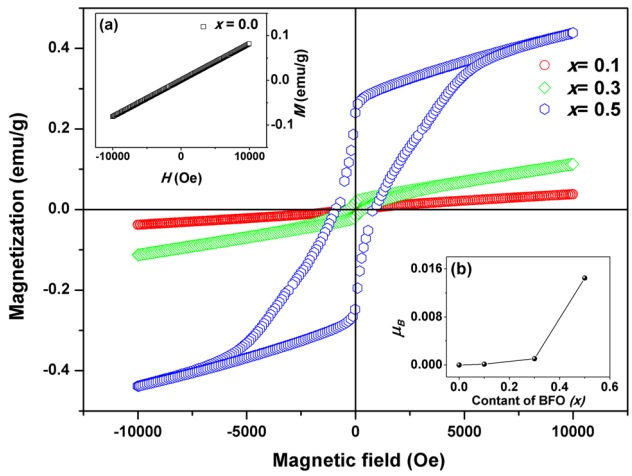

Fig. 6. Magnetization (M) versus applied magnetic field (H) for (1–*x*)BFT-*x*BFO ceramics. Insets: (a) M–H magnetic hysteresis loop of unmodified ceramic, and (b) magnetic moment (μ_B) as function of BFO content.

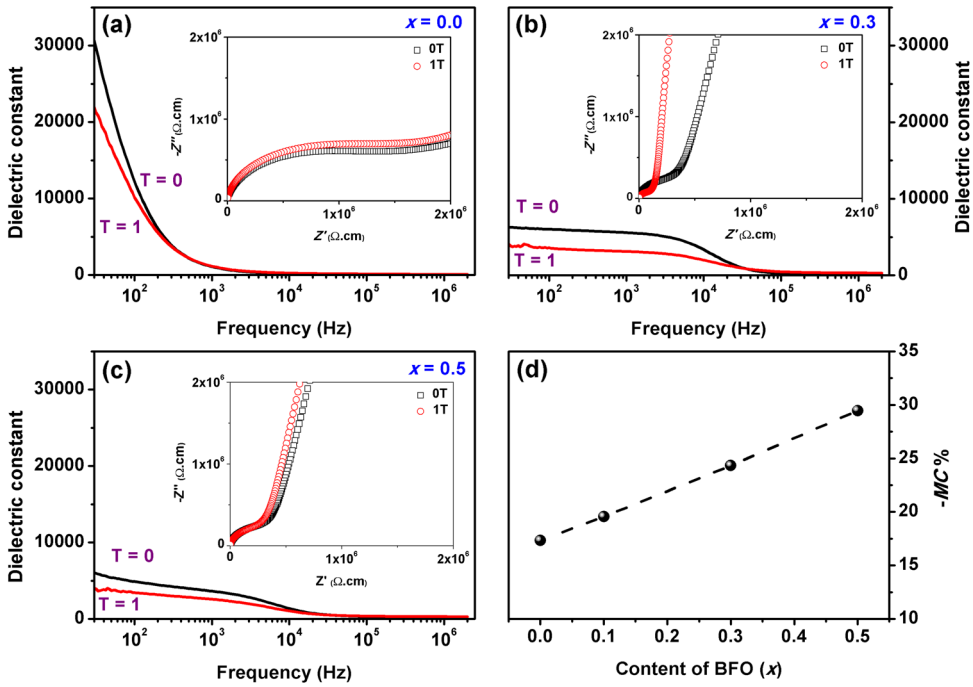

Fig. 7. (a–c) Dielectric constant versus frequency for x = 0, 0.3, and 0.5 ceramics at RT and (d) −MC versus BFO content. Insets show Z^* plots for the studied ceramics with and without applied magnetic field.

In this work, the capacitances of the bulk grain and grain boundary responses for all the ceramics were 1.1 pF/cm to 3.8 pF/cm (at −40°C) and 0.2 nF/cm to 2.8 nF/cm (at 300°C), respectively. However, the diameter of each arc changed when adding BFO. This suggests that there is a change in the resistance corresponding to each Z^* arc for the modified ceramics. After applying a magnetic field, the diameter of each arc also changed. Therefore, the resistances corresponding to each arc changed under an applied magnetic field, indicating that each conduction region presented a magnetoresistance (MR) effect.[45] Normally, the dielectric constant behavior of many materials can be related to the Maxwell–Wagner (MW) mechanism.[40] Furthermore, the change in resistance for each conduction region often results in a change of the ε_r value.[34] Therefore, a reason that explains the change in dielectric constant under an applied magnetic field is the MR effect along with the MW effect.[46,47]

CONCLUSIONS

$(1–x)Ba(Fe_{1/2}Ta_{1/2})O_3$-$xBiFeO_3$ [$(1–x)$BFT-xBFO] (x = 0.0, 0.1, 0.3, 0.5) powders were synthesized by a modified two-step calcination technique, and ceramics were fabricated by the conventional technique. The modified ceramics contained a mixture of BFT cubic phase and BFO rhombohedral phase. The modified ceramics also presented coarser grains compared with the unmodified ceramic. High thermal and frequency stability of ε_r were observed for the modified ceramics, while the dielectric constants of these ceramics remained high. BFO addition improved the tan δ value of the ceramics, as well as their magnetic properties. All ceramics presented the magnetocapacitance (MC) effect, which can be related to the magnetoresistance (MR) effect combined with the Maxwell–Wagner (MW) mechanism effect.

ACKNOWLEDGEMENTS

This work was supported by the Thailand Research Fund (TRF, BRG5680002, IRG5780013), National Research Council of Thailand, the National Research University Project under Thailand's Office of the Higher Education Commission, and CMU 50th anniversary Ph.D. Grant from Chiang Mai University. The Department of Physics and Materials Science, Faculty of Science, Graduate School of Chiang Mai University and the Science and Technology Research Institute, Chiang Mai University, Thailand are also acknowledged.

REFERENCES

1. A. Dutta and T.P. Sinha, *Mater. Res. Bull.* 46, 518 (2011).
2. Z. Wang, X.M. Chen, L. Ni, Y.Y. Liu, and X.Q. Liu, *Appl. Phys. Lett.* 90, 102905 (2007).
3. W.H. Jung, J.H. Lee, J.H. Sohn, H.D. Nam, and S.H. Cho, *Mater. Lett.* 56, 334 (2002).
4. C.Y. Chung and Y.H. Chang, *J. Appl. Phys*. 96, 6624 (2004).
5. S. Saha and T.P. Sinha, *J. Appl. Phys*. 99, 014109 (2006).
6. T. Phatungthane, G. Rujijanagul, K. Pengpat, S. Eitssayeam, T. Tunkasiri, L.F. Cotica, R. Guo, and A.S. Bhalla, *Curr. Appl. Phys*. 14, 1819 (2014).
7. Y.L. Chai, C.S. His, Y.T. Lin, and Y.S. Chang, *J. Alloys Compd*. 588, 248 (2014).
8. G. Li, S. Liu, F. Liao, S. Tian, X. Jing, J. Lin, Y. Uesu, K. Kohn, K. Saitoh, M. Terauchi, N. Di, and Z. Cheng, *J. Solid State Chem.* 177, 1695 (2004).

9. C. Chen, J. Cheng, S. Yu, L. Che, and Z. Meng, *J. Cryst. Growth* 291, 135 (2006).
10. Y. Du, Z.X. Cheng, X.L. Wang, P. Liu, and S.X. Dou, *J. Appl. Phys.* 109, 07B507 (2011).
11. R.E. Melgarejo, M.S. Tomar, R. Guzman, and S.P. Singh, *Ferroelectrics* 324, 101 (2005).
12. M.Y. Shami, M.S. Awan, and M.A. Rehman, *J. Alloys Compd.* 509, 10139 (2011).
13. W. Cai, S. Zhong, C. Fu, G. Chen, and X. Deng, *Mater. Res. Bull.* 50, 259 (2014).
14. X.J. Xi, S.Y. Wang, W.F. Liu, H.J. Wang, F. Guo, X. Wang, J. Gao, and D.J. Li, *J. Magn. Magn. Mater.* 355, 259 (2014).
15. H. Shokrollahi, *Powder. Technol.* 235, 953 (2013).
16. M.S. Bernardo, T. Jardiel, M. Peiteado, A.C. Caballero, and M. Villegas, *J. Alloys Compd.* 509, 7290 (2011).
17. G. Catalan and J.F. Scott, *Adv. Mater.* 21, 2463 (2009).
18. W.N. Su, D.H. Wang, Q.Q. Cao, Z.D. Han, J. Yin, J.R. Zhang, and Y.W. Du, *Appl. Phys. Lett.* 91, 092905 (2007).
19. S. Godara and B. Kumar, *Ceram. Int.* 41, 6912 (2015).
20. K. Chakrabarti, B. Sarkar, V.D. Ashok, S.S. Chaudhuri, and S.K. De, *J. Magn. Magn. Mater.* 381, 271 (2015).
21. D. Lin, K.W. Kwok, and H.L.W. Chan, *Ceram. Int.* 40, 1335 (2014).
22. V.F. Freitas, L.F. Cótica, I.A. Santos, D. Garcia, and J.A. Eiras, *J. Eur. Ceram. Soc.* 31, 2965 (2011).
23. R.N.P. Choudhary, K. Perez, P. Bhattacharya, and R.S. Katiyar, *Mater. Chem. Phys.* 105, 286 (2007).
24. E.V. Ramana, S.V. Suryanarayana, and T.B. Sankaram, *Solid State Sci.* 12, 956 (2010).
25. Q. Hang, Z. Xing, X. Zhu, M. Yu, Y. Song, J. Zhu, and Z. Liu, *Ceram. Int.* 38S, S411 (2012).
26. S. Sharma, V. Singh, R.K. Dwivedi, R. Ranjan, A. Anshul, S.S. Amritphale, and N. Chandra, *J. Appl. Phys.* 115, 224106 (2014).
27. K. Sanjoom and G. Rujijanagul, *Ferroelectrics*, 454, 51 (2013).
28. N. Itoh, T. Shimura, W. Sakamoto, and T. Yogo, *Ferroelectrics*, 356, 19 (2007).
29. I.P. Raevski, S.A. Prosandeev, A.S. Bogatin, M.A. Malitskaya, and L. Jastrabik, *J. Appl. Phys.* 93, 4130 (2003).
30. A.A. Zatsiupa, L.A. Bashkirov, I.O. Troyanchuk, G.S. Petrov, A.I. Galyas, L.S. Lobanovsky, and S.V. Truhanov, *J. Solid State Chem.* 212, 147 (2014).
31. J.K. Kim, S.S. Kim, and W.J. Kim, *Mater. Lett.* 59, 4006 (2005).
32. M. Sakar, S. Balakumar, P. Saravanan, and S.N. Jaisankar, *Mater. Res. Bull.* 48, 2878 (2013).
33. X. Chao, Z. Yang, Z. Li, and Y. Li, *J. Alloys Compd.* 518, 1 (2012).
34. K. Sanjoom, K. Pengpat, S. Eitssayeam, T. Tunkasiri, and G. Rujijanagul, *Phys. Status Solidi A* 211, 1720 (2014).
35. K. Singh, S.A. Band, and W.K. Kinge, *Ferroelectrics* 306, 179 (2004).
36. R.K. Dwivedi, D. Kumar, and O. Parkash, *J. Phys. D Appl. Phys.* 33, 88 (2000).
37. W. Xia, C.C. Wang, P. Liu, J.L. Ye, and W. Ni, *Curr. Appl. Phys.* 13, 1743 (2013).
38. Y.Y. Liu, X.M. Chen, X.Q. Liu, and L. Li, *Appl. Phys. Lett.* 90, 192905 (2007).
39. F.D. Morrison, D.C. Sinclair, and A.R. West, *J. Am. Ceram. Soc.* 84, 531 (2001).
40. Y.J. Li, X.M. Chen, R.Z. Hou, and Y.H. Tang, *Solid State Commun.* 137, 120 (2006).
41. P. Sharma and V. Verma, *J. Magn. Magn. Mater.* 374, 18 (2015).
42. H. Yan, F. Inam, G. Viola, H. Ning, H. Zhang, Q. Jiang, T. Zeng, Z. Gao, and M.J. Reece, *J. Adv. Dielectr.* 1, 107 (2011).
43. M. Rawat and K.L. Yadav, *J. Alloys Compd.* 597, 188 (2014).
44. J. Rani, K.L. Yadav, and S. Prakash, *Mater. Res. Bull.* 60, 367 (2014).
45. G. Catalan, *Appl. Phys. Lett.* 88, 102902 (2006).
46. Q. Fu, F. Xue, Z. Zheng, D. Zhou, L. Zhou, Y. Tian, and Y. Hu, *Ceram. Int.* 41, 4050 (2015).
47. P.K. Patel, K.L. Yadav, H. Singh, and A.K. Yadav, *J. Alloys Compd.* 591, 224 (2014).